Effects of plan area densities of cubical roughness elements on turbulent boundary layers

L. PERRET[a], T. PIQUET[b], J. BASLEY[c], R MATHIS[d]

a. LHEEA, UMR CNRS 6598, Centrale Nantes, Nantes, France, laurent.perret@ec-nantes.fr
b. LHEEA, UMR CNRS 6598, Centrale Nantes, Nantes, France, thibaud.piquet@ec-nantes.fr
c. LHEEA, UMR CNRS 6598, Centrale Nantes, Nantes, France, jeremy.basley@ec-nantes.fr
d. IMFT, UMR CNRS 5502, INPT, UPS, Toulouse, France, romain.mathis@imft.fr

Résumé

L'étude proposée ici s'intéresse à l'influence de la configuration géométrique des élements de rugosité disposés en paroi sur le développement d'une couche limite turbulente. Ce travail s'inscrit dans un contexte d'étude des écoulements atmosphériques se developpant au-dessus d'un milieu urbain. En se basant sur trois densités au sol d'obstacles cubiques et deux vitesses d'écoulement, six configurations d'écoulements sont étudiées. Celles-ci sont choisies de manières à être représentatives des trois régimes d'écoulements de canopée urbaine typiques observés et rapportés dans la littérature (régime de sillage isolé, sillages en interaction et écoulement affleurant). En se basant sur des mesures par anémométrie fil-chaud de la composante longitudinale de la vitesse, une étude détaillée des caractéristiques des couches limites générées est proposée. Une attention particulière a été accordée aux échelles caractéristiques de vitesse et de longueur permettant une bonne correspondance des statistiques obtenues dans les six configurations d'écoulement. Mise à part la vitesse moyenne, aucune des combinaisons de variables testées n'a permis la prise en compte satisfaisante des effets de changement de densité au sol d'obstacles. L'analyse a été complétée par l'étude des spectres temporels ainsi que l'évolution fréquentielle du maximum d'énergie de ces spectres. Ceci a permis d'identifier trois régions distinctes, dans lesquelles différents jeux de variables peuvent être utilisés. L'impact de la densité des obstacles sur les caractéristiques et la dynamique des écoulements est également confirmée. Cela suggère notamment l'existence d'interactions complexes entre les échelles générées dans la région proche du sommet des obstacles et celles existant dans la couche limite se développant au-dessus.

Abstract

Using detailed wind-tunnel hot-wire measurements of the streamwise velocity with three wall-roughness configurations and two flow velocities, the influence of the packing density of cubical roughness elements onto the characteristics of the turbulent boundary layer developing above is investigated. The plan area or packing density of the roughness obstacles, their arrangements and the ratio between their height and the obtained boundary layer thickness are representative of the lower-part of the atmospheric boundary layer developing over urbain terrains. In particular, three packing densities have been chosen to obtain the three near-wall flow regimes observed in urban canopy flows, namely isolated, wake interference and skimming flow regime. Through the investigation of wall-normal profiles of the mean, the variance and the skewness of the streamwise velocity, finding a unique set of variables enabling the collapse of the statistics obtained for the three roughness configurations has proved to be yet unsatisfactory,

except for the mean velocity. The investigation of wall-normal profiles of the streamwise vleocity component has shown that apart from the mean profile, no scaling exists for higher statistics. The analysis of the wall-normal evolution of energy spectrum and the temporal frequency corresponding to the peak in the pre-multiplied energy spectrum at each wall-normal location shows that the flow can be roughly divided into three main regions in which different scaling apply. It also demonstrates the influence of the roughness packing density on the flow regime and its dynamics, suggesting complex interactions between the near-wall scales and those from the overlying boundary layer.

Mots clefs : Couche limite atmosphérique urbaine ; Soufflerie ; Fil chaud

1 Introduction

During the past few years, large-scale motions (LSM) in turbulent boundary layers over smooth-walls have received renewed attention from the research community. Common features of the LSMs found in wall-bounded flows are that they consist in elongated low- and high-speed regions, the length of which scale with the boundary-layer depth (δ) and can reach several times δ, they populate the log- and outer layer, they are animated by a meandering motion in the horizontal plane [1] and interact with near-wall turbulence through an amplitude-modulation mechanism [2]. At the same time, attention has been devoted to the structure of boundary layer flows developing over rough walls, at laboratory scales or in the framework of atmospheric flows over urban or vegetation canopies, demonstrating similarities between flows over smooth and rough wall. In particular, the presence of streaky patterns of low- and high-speed regions, of ejection and sweep motions associated with the hairpin model and the organization of hairpin vortices in packets have been evidenced [3, 4, 5, 6]. The results obtained in flows over rough-walls suggest that, in spite of the strong disturbance of the flow at the wall, LSMs exist and interact with the canopy flow in a similar manner as in smooth wall boundary layers. However, in configurations representative of flows over urban canopies, it is likely that the arrangement, the shape and plan density of the roughness elements have a strong influence on the flow dynamics in the lower part of the boundary layer.

Building upon these recent results, the aim of the present work is to analyze the statistical and spectral characteristics of turbulent boundary layers developing over cubical roughness arrays of different plan densities, at high Reynolds number, which has never been fully properly documented. This study, conducted in an atmospheric wind tunnel, is based on single hot-wire measurements performed along a wall-normal profile across the boundary layer, in a flow configuration representative of the lower-part of the atmospheric boundary layer (ABL) developing over an urban canopy.

2 Experimental details

In this section, a description of the experimental apparatus and procedures and a presentation of the characteristics of the generated boundary layer are provided. In the following, x, y and z denote the streamwise, spanwise and wall-normal directions, respectively (figure 1), and u, v, w the streamwise, spanwise and wall-normal velocity components, respectively. Using the Reynolds decomposition, each instantaneous quantity u can be decomposed as $u = U + u'$ where U denotes the ensemble average (equivalent to a time-average) of u and u' its fluctuating part. The standard deviation of u is denoted as σ_u.

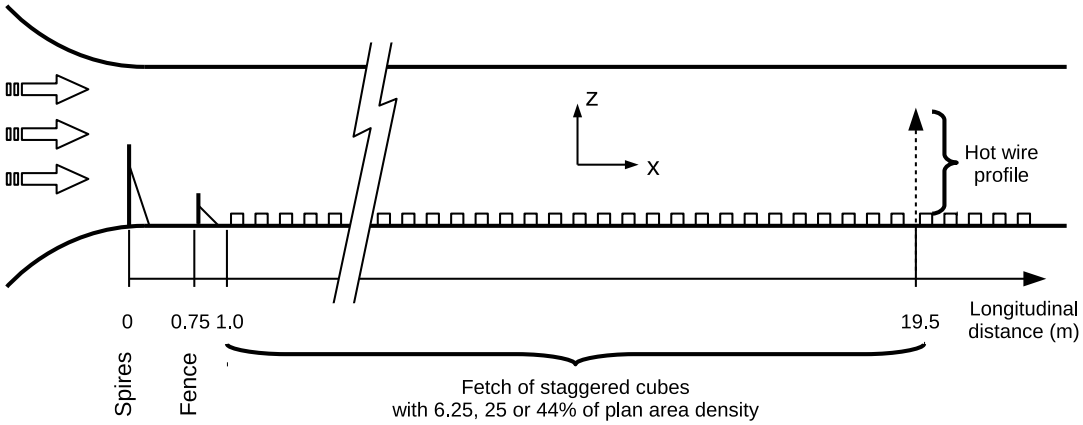

FIGURE 1 – Wind tunnel setup.

2.1 Experimental setup

Experiments were conducted in the atmospheric boundary layer wind tunnel of the Laboratoire de recherche en Hydrodynamique, Energétique et Environnement Atmosphérique of Ecole Centrale de Nantes (LHEEA, Nantes, France), which has working a section dimensions of 24 m $\times$ 2 m $\times$ 2 m. A reproduction of the lower-part of a suburban-type atmospheric boundary layer developing over an idealized urban canopy model was achieved by using three vertical, tapered spires of height of 800 mm and width of 134 mm at their base, a 200 mm high solid fence across the working section located 0.75 m downstream of the inlet, followed by a 22 m fetch of staggered cube roughness elements. The cube height was $h = 50$ mm. Three different rough walls of plan area density (i.e the ratio between A_p the area of the surface occupied by the roughness elements and that of the total surface A_T) of 6,25%, 25% and 44% were studied (figure 2). Experiments were systematically run at two nominal free-stream velocities U_e of 5.7 and 8.8 m/s, resulting in a total of 6 different flow configurations. The experiments were performed at a streamwise location of 19.5 m after the end of the contraction and consisted in single hot-wire measurements performed along a wall-normal profile across the boundary layer. A DISA 55M01 electronics associated to a DANTEC 55P11 single hot-wire probe (with a wire length of 1.25mm corresponding to $l^+ = 30$ to 56 wall units were used with overheat ratio set to 1.8. While these wire-length are in the upper range of advised length to avoid attenuation of the velocity flutuations and under-estimation of the variance in the near-wall region of flat-plate boundary layer flows [7], in the present case, this possible bias is not present as the presence of large roughness elements in the near-wall region shifts the whole spectral content toward the larger-scales. Near the top of the $\lambda_p = 25\%$ canopy, the Kolmogorov scale and Taylor micro-scale have been estimated, in wall-units, to be $\eta^+ \simeq 6$ and $\lambda_T^+ = 270$ [8] and the most energetic scales are of the order of $\lambda_{max}^+ = 1500$ (see Section 3.4). It ensures that, even if present, attenuation of the smaller scales remains marginal. At each wall-normal location in the profile, the hot-wire signal was sampled at 10 kHz over a period of at least 24 000 δ/U_e. An 8^{th} order anti-aliasing linear phase elliptic low-pass filter was employed prior signal digitization. A total of 39 logarithmically distributed wall-normal locations between 1.25 h and 1.3 δ and were investigated. Calibration of the hot-wire probe was performed at the begining of each half of each profiles by placing the probe in the free-stream flow. The calibration procedure was based on King's law and account for temperature correction using the method proposed by [9]. Static pressure, relative humidity and temperature in the wind tunnel were systematically recorded during the entire measurement period. Non dimensional pressure

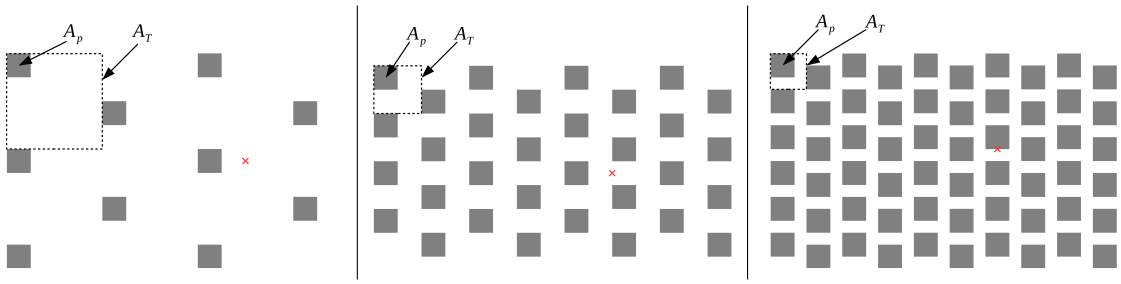

FIGURE 2 – Investigated canopy configurations with (left) $\lambda_p = 6.25\%$, (center) $\lambda_p = 25\%$ and (right) $\lambda_p = 44\%$. Red cross ($\times$) : location of the hot-wire profile kept constant relatively to the upstream cube ($1h$ downstream of the downstream edge).

TABLE 1 – Characteristics of the boundary layer.

Symbols	λ_p (%)	U_e (m/s)	u_*/U_e	δ/h	h^+	δ^+	d/h	z_0/h
○	6.25	5.65	0.065	22.4	1330	29700	0.52	0.08
●	6.25	8.80	0.066	21.5	2110	45500	0.52	0.09
△	25	5.77	0.073	22.7	1430	32400	0.59	0.11
▲	25	8.93	0.076	22.1	2260	49900	0.59	0.12
▽	44	5.55	0.064	21.0	1170	24600	0.77	?.??
▼	44	8.74	0.060	22.1	1840	40700	0.77	0.04

gradient $K = \frac{\nu}{\rho U_e^3}\frac{dP}{dx}$ along the wind-tunnel in the measurement cross-section was measured and found to be below -2.5 10^{-8}, which indicates a negligible influence of the pressure gradient on the streamwise boundary layer development [10]. Distribution of the wall pressure on the back and front faces of a cube obstacle was also measured for the six configurations. To this end, a cube face was equiped with 36 pressure ports to measure the pressure difference between the wall-pressure on the cube and the static pressure in the free-stream. The cube was rotated to access the pressure distribution on both faces successively. As detailed below, these pressure measurements were then used to estimated the displacement height d and the form drag.

2.2 Boundary layers characteristics

The main characteristics of the investigated boundary layers are shown in Table 1. In the following the superscript $^+$ denotes normalization based on the inner velocity and length scales u_* and ν/u_*, respectively. Below is described how they have been obtained. In the case of a turbulent rough-wall boundary layer, the mean velocity profile in the logarithmic region reads as :

$$U^+ = \frac{U}{u_*} = \frac{1}{\kappa}\ln\left(\frac{z-d}{z_0}\right) \quad (1)$$

$$= \frac{1}{\kappa}\ln(z-d)^+ + B - \Delta U^+ \quad (2)$$

where u_* is the friction velocity, κ is the von Kármán constant, B is the smooth-wall intercept, d the displacement height or zero-plane displacement, z_0 the roughness length in meteorology and ΔU^+ the velocity deficit (equivalent of $z_0^+ = z_0 u_*/\nu$ in the engineering community), these two being related by

$$\frac{1}{\kappa}\ln z_0^+ = -B + \Delta U^+ \quad (3)$$

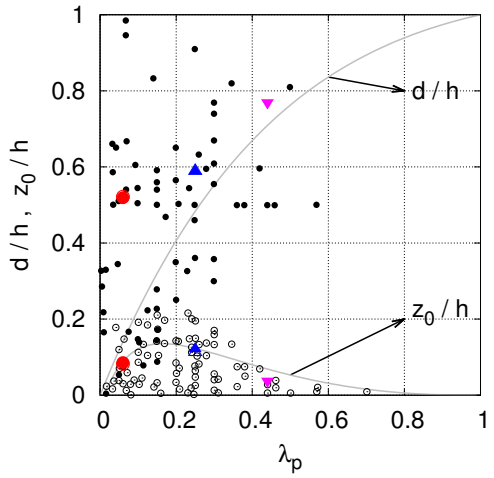

FIGURE 3 – Values of d/h and z_0/h as a function of λ_p of (colored symbols, as in Table 1) the present configurations and (solid and open black circles) from the compilation of wind tunnel performed by [14]. Models proposed by [13] are shown in gray solid lines.

In the present study, the expression of the mean velocity profile from the meteorology is retained and $\kappa = 0.4$. Besides the friction velocity u_*, d and z_0 are the key parameters to describe the influence of the rough wall onto the boundary layer flow from an aerodynamic point of view. As proposed by [11], the zero-plane displacement is interpreted as the height at which the drag on the roughness elements is exerted. In the case of large roughness elements, the contribution of the viscous force to the drag is negligible [12] with the form drag D being the major contributor. The zero-plane displacement can therefore be estimated directly from the calculation of the moment of the pressure forces on a roughness element about its base :

$$d.D_p = \int_{A_f} z(P_f - P_b)dS \tag{4}$$

where A_f is the frontal area of the cube, P_f and P_b the local pressure on the front and back of the cube, respectively and D_p, the pressure drag calculated as :

$$D_p = \int_{A_f} (P_f - P_b)dS \tag{5}$$

Being the velocity scale formed from the wall-stress, the friction velocity can also be estimated from the form drag as :

$$u_* = \sqrt{\frac{1}{\rho}\frac{D_p}{A_T}} \tag{6}$$

An alternative way is to perform the classical fitting procedure of the velocity profile in the log region with the relationships in eqn 2 and estimate both u_* and z_0 [12]. In the present study, d and u_* were estimated from the pressure measurements and z_0 from the fit of the velocity profile in the log region (Table 1). The boundary layer thickness δ, defined as the height where the mean velocity is equal to 99% of the free-stream velocity U_e, is also shown in Table 1.

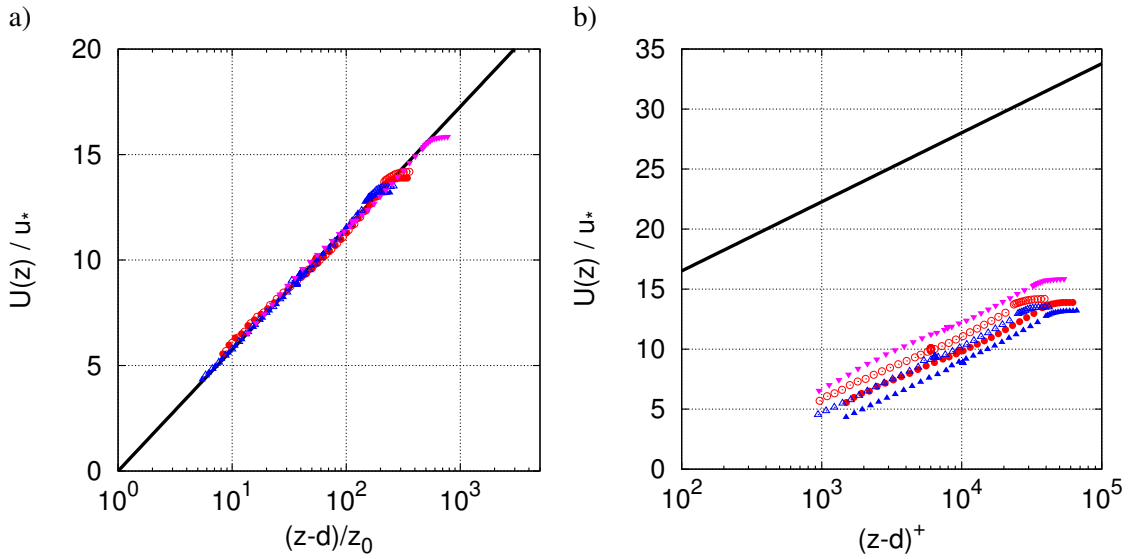

FIGURE 4 – Wall-Normal profile of the normalized mean streamwise velocity $U(z)/u_*$ as a function of (a) $(z-d)/z_0$ and (b) $(z-d)^+$. Symbols : see Table 1 ; black solid lines : logarithmic law from eqn 2 or for smooth wall boundary layers, for a) and b), respectively.

3 Results

3.1 Mean flow and aerodynamics parameters

Aerodynamics parameters d and z_0 estimated from the drag measurement and the mean velocity profile are compared to both the models derived by [13] and the data compiled by [14] in their extensive literature review (figure 3). It should be noted here that only wind tunnel data from the review of [14] are considered here and that they include configurations with different plan area density λ_p but also frontal area density. In the present study, because cubic obstacles are used, both parameters are equal. One should also keep in mind the wide spread of the data, traducing the difficulty in both obtaining accurate aerodynamics parameters and deriving relationships between them and simple morphologic parameters such as λ_p. Finally, it must be noted here that the three present configurations are representative of the three different near-wall flow regimes identified in the literature (6.25 % : isolated flow, 25 % : wake interference flow, 44 % : skimming flow) [14] and which result in the bell-shaped curve for the modelled relationships between z_0/h and λ_p [13]. One therefore can expect differences in flow dynamics in the near-wall region when the roughness morphology is varied.

Figure 4a, shows the mean velocity profile plotted using d and z_0 as scaling parameters, where, for all the configurations, a large portion of the profiles follows the logarithmic law. With this representation, no Reynolds number effect is visible. When scaling the wall-normal coordinate z in inner scales (figure 4b), the mean velocity profiles still clearly exhibit a well-defined large logarithmic region but also clearly show the influence of the roughness density. The roughness is responsible for a downward shift of the log-law region, and the higher z_0, the higher the velocity deficit ΔU^+ (defined here as the wall-normal distance between the smooth-wall logarithmic law and velocity profile in the logarithmic region), implying the break-down of the classical representation in inner scales if the velocity deficit is not accounted for (i.e the lack of universality of the velocity profile when Reynolds number and wall geometry are varied).

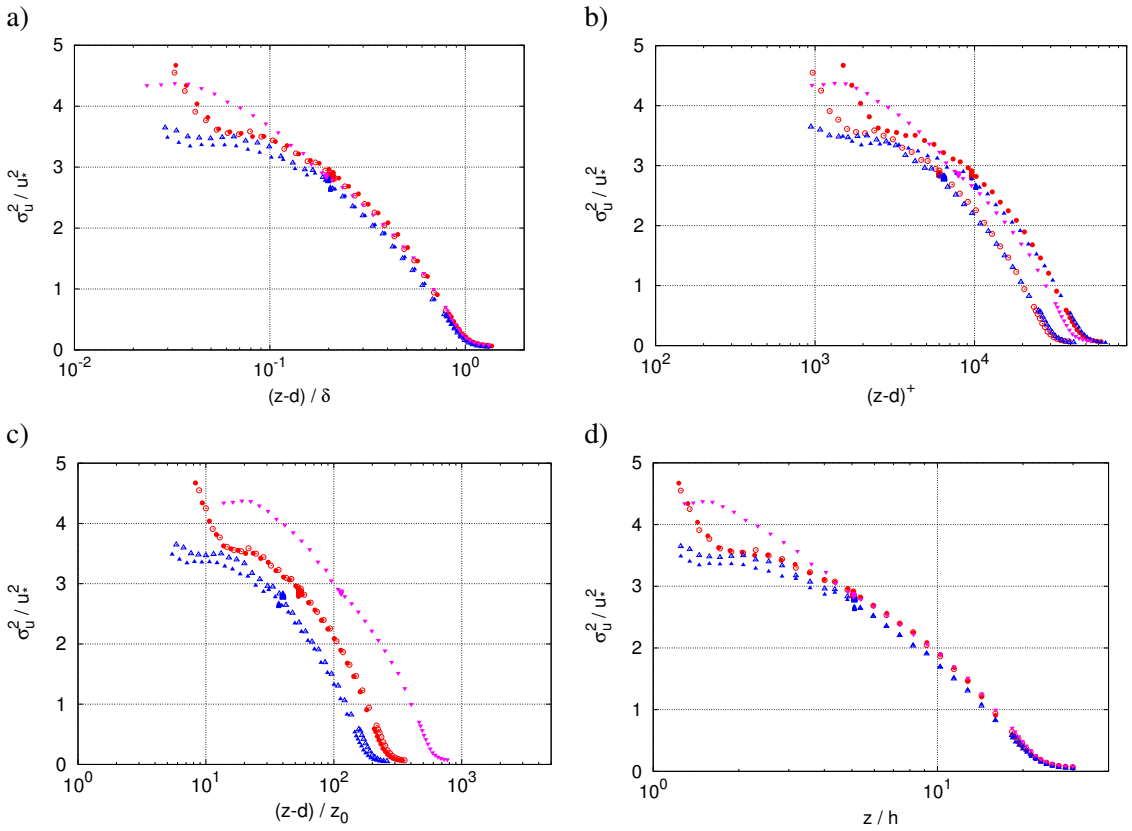

FIGURE 5 – Evolution of the normalized variance of the streamwise velocity σ_u^2/u_*^2 with the wall-normal location (a) in inner variables, (b) outer variables, (c) normalized using z_0 and (d) using the obstacle height h as the reference length scale. Symbols : see Table 1.

3.2 Variance of the streamwise velocity

In the present section, different scaling are tested to account for the influence of both Reynolds number and canopy configuration on the variance of the u. As found by [15] in their study of various rough wall at lower Reynolds number, a good collapse is obtained in the outer region when outer variables are used, i.e for $(z-d)/\delta > 0.1$ (figure 5a). Globally, the inner variables does not provide a good scaling, even close to the roughness elements (figure 5b). In the outer layer, this scaling fails at collapsing the different Reynolds numbers while a good collapse in found between the canopy configurations, which was to be expected as the flow far from the wall is becomes insensitive to the influence roughness elements. Using z_0 and d as a length-scale for the wall-normal location (figure 5c) also fails at collapsing all the variance profiles ; only a partial collapse between the canopies (all but the $\lambda_p = 44\%$ canopy) is obtained in a limited range $(z-d)/z_0 \simeq 20$. This last point can be explained by the very small variability of d and z_0 with regards to U_e. Finally, figure 5d shows profiles when scaled using the obstacle height h and not taking into account the zero-plane displacement d. A good collapse in the outer region is obtained, consistently with the very close ratio δ/h shown by the six configurations. The use of $(z-d)/h$ instead of z/h has no significant impact on the quality of the collapse. A good collapse is also obtained in the near-wall region for all the configurations but the $\lambda_p = 44\%$ canopy. Overall, no set of scaling variables has been found to satisfactorily collapse all the wall-normal profiles of variance of the six flow configurations.

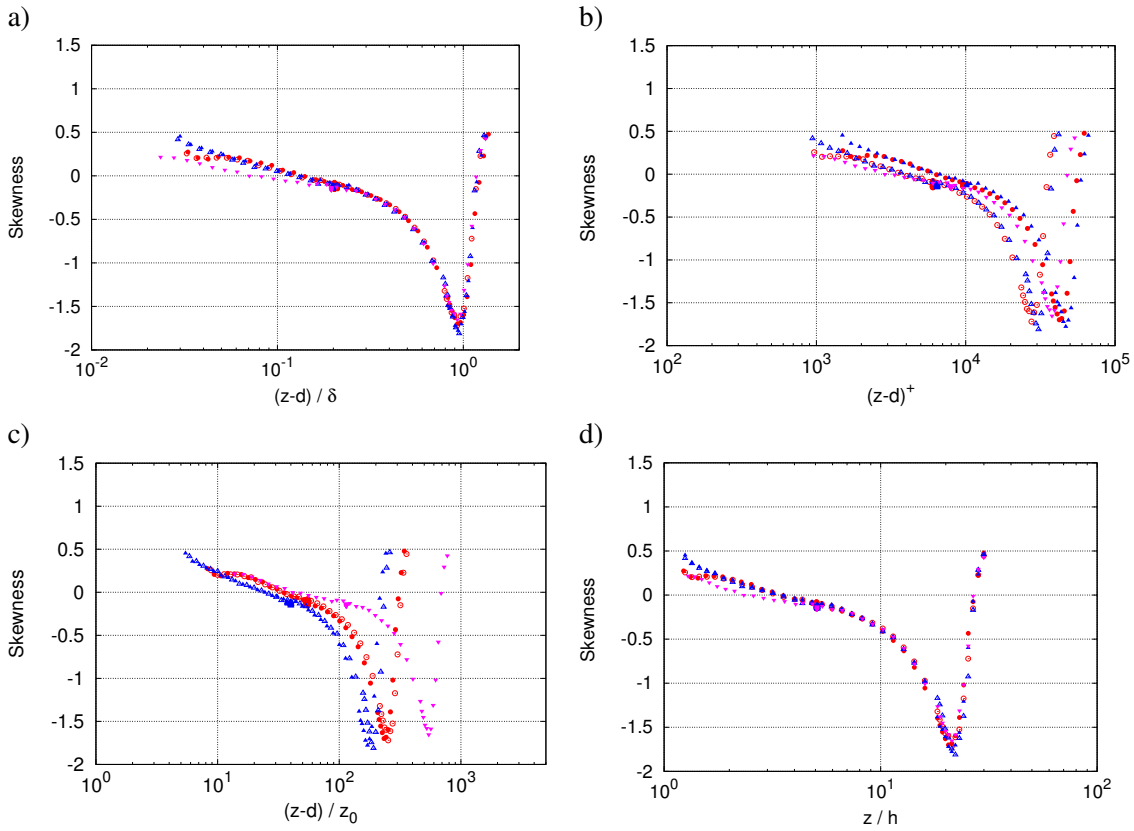

FIGURE 6 – Evolution of the skewness of the streamwise velocity with the wall-normal location (a) in inner variables, (b) outer variables, (c) normalized using z_0 and (d) using the obstacle height h as the reference length scale. Symbols : see Table 1.

3.3 Skewness of the streamwise velocity

The wall-normal evolution of the skewness of the streamwise velocity using different scaling of the wall-normal coordinate is shown in figure 6. In agreement with the literature of boundary layer flows over dense canopies [17], the skewness of u is positive just above the top of the obstacles, close to the Gaussian value of zero in the inertial layer region and becomes negative above, a classical behavior in the outer layer of boundary-layer flows [18]. As for the variance, the use of the outer variables (or the canopy height h for the reason evoked above) provides a good collapse of the outer region (figure 6a and d). In the near-wall region, inner variables $(z-d)^+$ allow for the correct collapse of the $\lambda_p = 6.25\%$ and $\lambda_p = 25\%$ configurations but not for both Reynolds numbers. The canopy with $\lambda_p = 44\%$ shows a different behavior (figure 6b). Figure 6c shows a good agreement between Reynolds numbers for a given roughness density when z_0 is used as length-scale. The $\lambda_p = 6.25\%$ and $\lambda_p = 44\%$ skewnesses collapse for only a limited range of height, i.e $15 < (z-d)/z_0 < 35$. Finally, using h as a scaling parameter allows for a good agreement for both Reynolds numbers canopy configuration for $\lambda_p = 6.25\%$ and 25% for all heights down to $z/h = 1.8$. The skewness profile of the configuration $\lambda_p = 44\%$ shows a departure from the two others below $z/h = 5$.

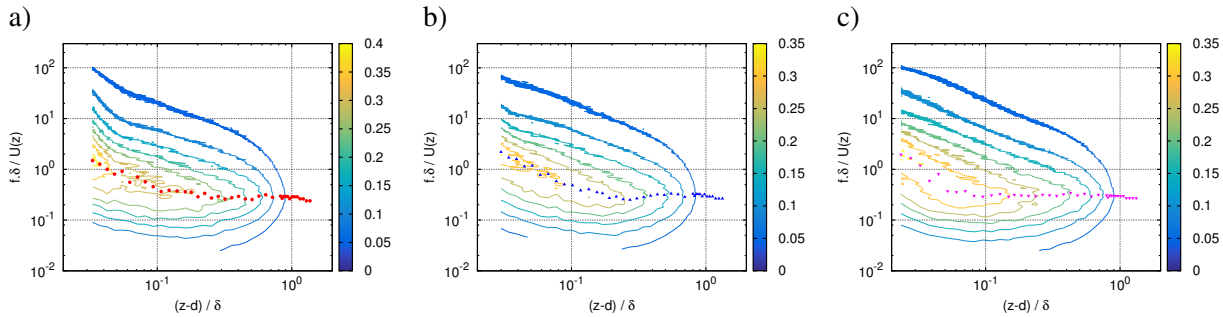

FIGURE 7 – Wall-Normal evolution (in outer-variables) of the pre-multiplied energy spectrum of the streamwise velocity at the highest Reynolds number for (a) $\lambda_p = 6.25\%$, (b) $\lambda_p = 25\%$ and (c) $\lambda_p = 44\%$ (note the difference in range of the color contours). The temporal frequency f is normalized by the boundary layer thickness δ and the local mean velocity $U(z)$ as $f\delta/U(z)$. Symbols show the location of the maximum of the pre-multiplied spectrum.

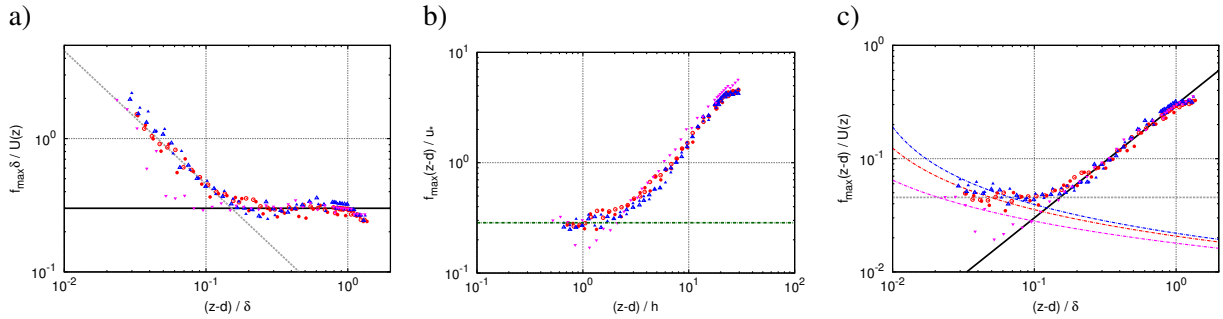

FIGURE 8 – Wall-Normal evolution of the frequency f_{max} corresponding to the peak of the pre-multiplied energy spectra of the streamwise velocity as shown in figure 7. Different length and velocity scales are used to scale both f_{max} and the wall-normal location z : a) $f_{max}\delta/U(z)$ vs $(z-d)/\delta$, b) $f_{max}(z-d)/u_*$ vs $(z-d)/h$ and c) $f_{max}(z-d)/U(z)$ vs $(z-d)/\delta$. The solid black line in a) corresponds to a value of $f_{max}\delta/U(z) = 0.3$; the green dash-dotted line in b) to $f_{max}(z-d)/u_* = 0.28$; the gray dashed line in c) to $f_{max}(z-d)/U(z) = 1/22$ (see text for more details).

3.4 Spectrum of the streamwise velocity

In order to study the relevant scales of most energetic structures, evolution with distance to the wall of the pre-multiplied energy spectra of the streamwise velocity is presented in figure 7. For the sake of brevity, only the highest Reynolds number is shown. In the outer region, the most energetic scales asymptotically tend to the same normalized frequency, for the three canopy configurations. The wall-normal extent of the region where these large-scales dominate depends nonetheless on the canopy density λ_p, the largest region being found for $\lambda_p = 44\%$ (figure 7c). Below that region, an increase of the frequency of the most energetic scales is observed, and reachs similar wavelength when the temporal frequencies are scaled using h and u_* (not shown). One can also note the difference in shape of the spectra at higher frequency close to the canopy top, suggesting a change in flow dynamics in the near-wall region. The evolution of the frequency f_{max} corresponding to the peak in the pre-multiplied spectrum is analysed in more details below, in terms of the relevant scaling variables for both the wall-normal location and the f_{max}.

An attempt at finding the relevant length and velocity scales corresponding to the frequency of the peak

observed in the spectra in figure 7 is presented in figure 8. Different regions of the flow are considered. In outer-region of the boundary-layer ($(z-d)/\delta > 0.2$), scaling is achieved with outer variables δ and the local mean velocity $U(z)$ (figure 8a), showing that in the logarithmic region and the outer region, the most energetic scales have a non-dimensionnal frequency $f_{max}\delta/U(z) = 0.3$ (solid black line in figure 8a and c) which corresponds to a wavelength $\lambda = U(z)/f \simeq 3.3\delta$, consistently with existing literature. This confirms the existence of large-scales structures whose length scales with δ that occupy most of the upper part of the boundary layer. The shape of the velocity spectra in the surface layer of the atmospheric boundary-layer over flat uniform terrain has been extensively studied [16]. Depending of the stability regime of the atmosphere, expressions have been derived to model the pre-multiplied spectrum $fS_u(f)$ as a function of the non-dimensionnal frequency $n = f(z-d)/U(z)$. It implies that in the surface layer, the spectrum and the most energetic scales scale with the wall-distance. The most commonly used for the streamwise velocity for a neutrally stable boundary-layer reads as [16] :

$$fS_u(f)/u_*^2 = 102n(1+33n)^{-5/3} \tag{7}$$

It can be shown that the modelled spectrum reaches its maximum for $n = 1/22$. This asymptotic value is represented as the gray dashed line in figure 8a and c. It can be seen that the agreement with the surface layer value $f(z-d)/U(z) = 1/22$ is good for a limited range of heights centered around $(z-d)/\delta = 0.1$, for the canopies with $\lambda_p = 6.25\%$ and 25%. In the near-wall region (figure 8b), the best collapse is achieved using u_* and $(z-d)$ as velocity and length scales to normalize f_{max} and the obstacle height h for the wall-distance $(z-d)$. Using these variables, a good agreement between the configurations with $\lambda_p = 6.25\%$ and 25% is obtained, resulting in a constant normalized frequency $f_{max}(z-d)/u_* = 0.28$ in the region where $(z-d)/h < 1$ (green dash-dotted line in figure 8b). This value has been estimated empirically and the link with relevant flow parameter is still to be made. A collapse of the configuration $\lambda_p = 44\%$ is only achieved for the lowest three points, the evolution of f_{max} for this case being notably different, therefore suggesting a thiner roughness sublayer and a dynamics in the lower boundary layer different from the two other configurations. This last finding is evidence of the change of flow regime mentionned during the analysis of the mean flow and of figure 4b, and qualitatively reported by [14]. These three different scalings, corresponding to three distinct regions, are shown in figure 8c in which the line $f(z-d)/U(z) = 1/22$ is now horizontal (grey dashed line) and scaling f_{max} with $(z-d)$ and $U(z)$ transforms the unique asymptote $f_{max}(z-d)/u_* = 0.28$ in the near-wall region as three different curves because of the dependence of u_* with λ_p. The three distinct regions, namely the near canopy-top, an intermediate region and the outer region are clearly visible. It is worth noting here that the departure from the outer region asymptote with decreasing height corresponds to the point where the skewness of u switches from negative to positive values (figure 6a). Regarding the $\lambda_p = 44\%$ canopy, this departure happens considerably lower than for the others with a collapse onto the asymptote $f_{max}(z-d)/u_* = 0.28$ (purple dash-dotted line) of the three lowest points in the near canopy-top region.

4 Conclusions

The influence of the roughness geometry on the characteristics of an atmospheric boundary layer has been investigated using hot-wire measurements of the streamwise velocity. The investigated flow configurations are representative of the lower atmosphere developing over urban-like terrain, for which the plan area density λ_p has been varied to investigate the three typical near-wall flow regime identified

in the literature (i.e isolated, wake interference and skimming flow regime) [14]. The present study has focussed on the identification of the relevant length and velocity scales that can be used to scale the characteristics of the streamwise velocity depending on the considered flow region. Concerning the wall-normal profiles of the streamwise velocity, in agreement with previous works performed on similar flow configuration, u_*, d and z_0 have been found to be the best set of parameters to collapse all the flow configurations, taking into account both Reynolds number effects and the influence of λ_p. Conversely, when considering the profiles of the variance of u, the use of these variables did not enable the collapse of the roughness configurations, only being able to account for the Reynolds number variation. The use of the outer variable δ enables a reasonnably good collapse in the outer region of the boundary layer, as well as the obstacle height h. The relative success of employing h as scaling variable is attributed to the fact that, for the present configurations, the ratio δ/h is very similar. The use of inner variables allowed for a reasonnable collapse in a very limited range of heights $(z-d)^+$ close to the wall for two of the roughness configurations ($\lambda_p = 6.25\%$ and 25%) but failed with the most dense canopy ($\lambda_p = 44\%$). The use of δ to scale the wall distance $(z-d)$ enabled a good collapse of the skewness profiles in the outer region, for the three canopy density. A good match of the skewness profiles of the configurations $\lambda_p = 6.25\%$ and 25% has in fact been obtained in most of the boundary layer, except in the near-wall region. Departure from this good collapse is observed for the configuration $\lambda_p = 44\%$. None of the other tested scaling were able to provide a good match of all the configurations in the lowest region of the flow. Investigation of the wall-normal evolution of the pre-multiplied energy spectra and that of the frequency $f_{max}(z)$ of the local energy peak clearly evidenced the existence of three distinct regions corresponding to three different set of scaling variables. A link between the change of sign of the skewness and the transition from the outer region and the so-called intermediate region has also been evidenced.

In the present study, thanks to an adequate choice of the roughness configurations, the change in the near-canopy flow regime (i.e isolated, wake interference and skimming flow regime) qualitatively reported in the literature [14], has been quantified and observed to leave its imprint onto most of the statistics of u, including the most energetic frequencies in the spectrum, therefore suggesting a complex interaction between the most energetic scales generated close to the canopy and those existing in the overlying boundary-layer. Investigating this scale interplay is the subject of ongoing research efforts.

Acknowledgments

The authors acknowledge the financial support of the French National Research Agency through the research grant URBANTURB N o ANR-14-CE22-0012-01.

Références

[1] N. Hutchins, I. Marusic, Evidence of very long meandering features in the logarithmic region of turbulent boundary layers, J Fluid Mech, 579 (2007) 1–28.

[2] R. Mathis, N. Hutchins, I. Marusic, Large-scale amplitude modulation of the small-scale structures in turbulent boundary layers, J Fluid Mech, 628 (2009) 311–337.

[3] J. Jiménez, Turbulent flow over rough walls, Annu Rev Fluid Mech, 36 (2004) 173–196.

[4] J.J. Finnigan, R.H. Shaw, E.G. Patton, Turbulence structure above a vegetation canopy, J Fluid Mech, 637 (2009) 387–424.

[5] A. Inagaki, M. Kanda, Organized structure of active turbulence over an array of cubes within the logarithmic layer of atmospheric flow, Boundary-Layer Meteorol, 135 (2010) 135–228.

[6] H. Takimoto, A. Sato, J. F. Barlow, R. Moriwaki, A. Inagaki, S. Onomura, M. Kanda, Particle image velocimetry measurements of turbulent flow within outdoor and indoor urban scale models and flushing motions in urban canopy layers, Boundary Layer Meteorol, 140 (2011) 295–314.

[7] N. Hutchins, T.B. Nickels, I. Marusic, M.S. Chong, Hot-wire spatial resolution issues in wall-bounded turbulence, J Fluid Mech, 635 (2009) 103–136.

[8] K. Blackman, L. Perret, I. Calmet, C. Rivet, Turbulent kinetic energy budget in the boundary layer developing over an Urban-like rough wall using PIV, Phys Fluids, *Submitted*, 1–51.

[9] M. Hultmark, A. J. Smits, Temperature corrections for constant temperature and constant current hot-wire anemometers, Meas Sci Technol, 21 (2010) 1–4.

[10] D.B. DeGraaff, J.K. Eaton, Reynolds-number scaling of the flat-plate turbulent boundary layer, J Fluid Mech, 422 (2000) 319–346.

[11] P.S. Jackson, On the displacement height in the logarithmic velocity profile, J Fluid Mech, 111 (1981) 15–25.

[12] H. Cheng, I.P. Castro, Near wall flow over urban like roughness, Boundary Layer Meteorol, 104 (2002) 229–259.

[13] R.W. MacDonald, R.F. Griffiths, D.J. Halls, An improved mehtod for the estimation of surface roughness of obstacles arrays, Atm Env, 32 (1998) 1857–1964.

[14] C.S.B. Grimmond, T.R. Oke, Aerodynamic properties of urban areas derived from analysis of surface form, J Appl Meteorol, 38 (1999) 1262–1292.

[15] K.A. Flack, M.P. Schultz, J.S. Connelly, Examination of a critical roughness height for outer layer similarity, Phys Fluids, 19 (2007) 1–10.

[16] J.C. Kaimal, J.J. Finnigan, Atmospheric boundary layer flows—their structure and measurement, Oxford University press (1994).

[17] J.J. Finnigan, Turbulence in plant canopies, Annu Rev Fluid Mech, 32 (2000) 519–571.

[18] R. Mathis, N. Hutchins, I. Marusic, A predictive inner–outer model for streamwise turbulence statistics in wall-bounded flows, J Fluid Mech, 681 (2011) 537–566.